2016 NDIA GROUND VEHICLE SYSTEMS ENGINEERING AND TECHNOLOGY SYMPOSIUM
POWER & MOBILITY (P&M) TECHNICAL SESSION
AUGUST 2-4, 2016 - NOVI, MICHIGAN

ENABLING ELECTRIFIED DIESEL ENGINE-POWERED AND VEHICLE-SUPPORTED MICROGRIDS

Rasoul Salehi
Jason Martz
Anna Stefanopoulou
Department of Mechanical Engineering
University of Michigan
Ann Arbor, MI

Denise Rizzo
Dean McGrew
US Army, TARDEC
Warren, MI

Taylor Hansen
Controlled Power Technologies
Southfield,MI

ABSTRACT

A sudden increase in microgrid electrical power consumption requires the fast supply of energy from different generating sources to guarantee microgrid voltage stability. This paper presents the results of simulations investigating the integration of an electric supercharger into a Heavy Duty Diesel (HDD) genset connected to a microgrid for reducing engine speed droop in response to an abrupt power demand requested from the grid. First, a mean value model for the 13 L HDD engine is used to study the response of the baseline turbocharged engine during a fast load increase at low engine speed. The limited air mass in the cylinder during the transient results in engine lugging and ultimately engine stall. Then, an electrical supercharger is integrated before the turbocharger compressor to increase the engine air charge. During steady state operation, the simulation results indicate that the supercharger is able to increase the air-charge by approximately 50% over the lower half of the engine map, which is the key area of interest for load acceptance as it restricts the HDD response during fast power requests. Then, the supercharged engine is tested with abrupt power disturbances applied at engine idle. The results show the ability of the supercharger to mitigate engine speed droop, reducing it from 180 RPM to less than 30 RPM. Strategies are also shown where the supercharger can increase the engine's load acceptance ability without increasing fuel consumption compared to strategies such as increased engine idle speed.

INTRODUCTION

Electrified auxiliary systems, electrical export power systems, advanced energy weapons systems and electronic armor solutions all require electrical power to function. One benefit (and liability) of electronic systems compared to their mechanical counterparts is their fast response to inputs. Electronic systems can be quickly loaded with short but high inrush currents. For example an electric motor's locked rotor current can be six times its continuous current and is supplied to the motor for the first milliseconds after it is accelerated quickly. Export power converters can load extremely quickly and transfer electrical power from a generator/storage to a user. However, this fast loading capability requires a grid with high inertia or a fast source of supply to provide voltage stability. In a microgrid (as shown in Figure 1) with low grid inertia, the inrush current can be supplied by (for example) uninterruptible power supply (UPS) units with storage devices. Engines with turbochargers are challenged to meet such sudden power demands, hence the UPS is typically sized to supply short term electrical loads, giving the diesel engine sufficient time to achieve the conditions necessary for generating the demanded power [1, 2]. The amount of power required in the initial seconds after the electrical device initialization defines the size and cost of the UPS units. Therefore, reducing the time required to increase the power output of a

diesel engine decreases the dependency of the grid on the UPS and consequently the grid cost and weight.

The rate of torque increase in a diesel engine is constrained by the air-fuel ratio, which dictates exhaust gas temperature and smoke limits. In extreme conditions, an engine stall occurs if the load demand is too abrupt and the air-charge system cannot respond. This paper investigates the integration of an electrical supercharger (eSC) into a heavy duty diesel (HDD) engine to enable more rapid engine load transition from idle to near full loads. Smart/electrified superchargers provide a means for improving engine load acceptance capability required for mobility and fast loading of electrified microgrid sub-systems [3, 4]. This study will utilize the Detroit Diesel DD13 HDD engine, which is in wide use within the Army fleet, including several M915 heavy truck variants such as the M915A2, M915A3, M916A1 and M916A2. However, such a solution could be applied to other military generator and vehicle systems, for both new engines and as a retrofit option.

The paper simulates the integration of an eSC into a DD13 HDD engine mean value model. The eSC is used to reduce the engine air-charge delay and improve engine transient response, which is constrained by a fuel limiter which prevents low air-fuel ratio excursions that generate excessive smoke. First, the engine microgrid integration is described and modeled. Next, the baseline diesel engine response to a rapid power disturbance is studied. Finally, the engine power response is studied with an eSC integrated into the engine air-charge path.

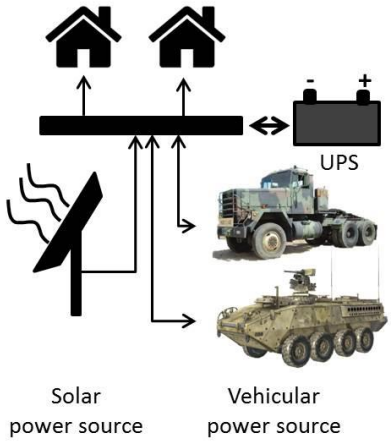

Figure 1- Example microgrid elements.

MODELING DIESEL ENGINE POWERED ELECTRIC GENERATOR

Engine Connection to a Microgrid

Figure 2 shows how the engine mechanical power is transferred to the microgrid as electricity. The power requirement for on-site electrical equipment and the vehicle's auxiliary systems electrification is much more than low voltage electrical power generation systems can provide (~75kW required for electrification of the Stryker which is >5kAmps at 14V). In addition, high voltage systems are much more power dense than low voltage ones[5] and have the potential to generate nearly 10x the power for the same weight and space as a low voltage system (see for example the Ragone plot in [6]). Therefore, given the extremely limited packaging space available on military vehicles, electrification at higher voltages is required. Shown by the schematic in Figure 2, the vehicle engine is attached to a 600 V DC generator which feeds current to the DC/DC or DC/AC convertors. The converters regulate their input voltage level based on the end user requirements. The generator torque (applied to the engine) is adjusted such that it accounts for any changes in the grid power (PW_L).

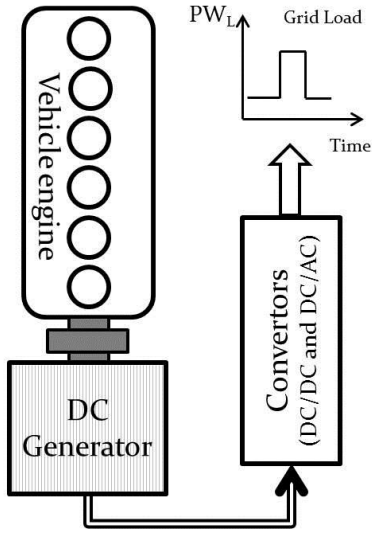

Figure 2- HDD engine connection to the microgrid.

Supercharged HDD Engine Model

A model of the 12.8 L heavy duty diesel (HDD) DD13 engine is used in the current work for studying the effect of the eSC on the engine torque (and power) response. The turbocharged (TC) engine is equipped with an asymmetric twin-scroll turbine, where the exhaust manifold is constructed so that the flow from three of the cylinders feeds into a small turbine scroll while the flow from the other three cylinders feeds into a larger scroll. This specific design of the exhaust manifold provides a fuel efficient way of creating high boost and EGR. The engine is also equipped with a pneumatic wastegate (WG) valve, which bypasses the large scroll to avoid over-boosting and to reduce pumping losses.

A high fidelity model for the HDD engine is used in this work for the purpose of eSC effect analysis. The baseline engine model is formed by connecting individual component models. Component models include the engine cylinder, turbocharger, intercooler, WG and EGR valves, which are included within dynamical models for the intake manifold pressure (P_{im}), large and small scroll exhaust manifold pressures (P_{eml} and P_{ems}), exhaust manifold pressure downstream of the turbine (P_{dst}), burned gas fractions in the intake and exhaust manifold (F_{im}, F_{em}) and turbocharger speed (N_{tc}). The model is required to accurately predict the engine performance both at steady engine operation and during a fast transient. Therefore, extensive steady state model identification and a secondary feedback calibration of model parameters are applied to ensure high model accuracy. Additional model details are presented in references [7-9]. The modular form of the engine model allows the addition of new component sub-models (here the electric supercharger sub-model) to the baseline engine model.

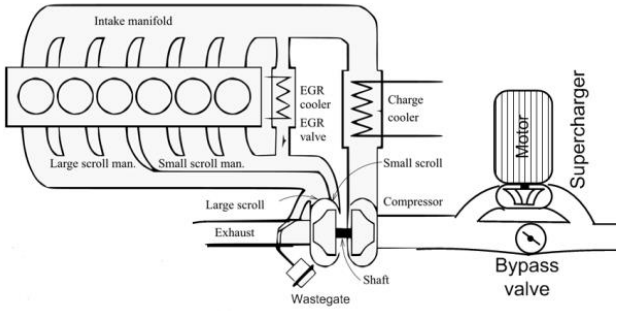

Figure 3- Supercharged HDD engine schematic.

Figure 4 shows the model's ability to predict the measured data (including T_e (the engine torque), P_{im} and N_{tc}) at different engine speeds (N_e) with ±5% accuracy. Since this paper also studies transients at low engine speeds, additional model validation is presented in Figure 5 for a fast pedal tip-in, with load transitioning from 0 to 80% at constant engine speed. The results show a 5% match between measured and estimated T_e, P_{im} and N_{tc}.

After validating the engine model, the WG and EGR valves are kept closed in the low engine speed simulations of this work. Also, a proportional-integral (PI) controller adjusts the fuel injection rate ($\dot{m}_f$) to control the engine speed. The engine model also includes a fuel limiter to limit the injected fuel mass to maintain the equivalence air fuel ratio (λ) above the smoke limit (as λ_{crit}), which is chosen as $\lambda_{crit} = 1.6$ [11]. Finally a torque limiter is applied to limit the engine torque to a maximum of 2000 Nm (similar to the DD13 peak torque) at all speeds avoiding mechanical damage that might happen at extreme torques.

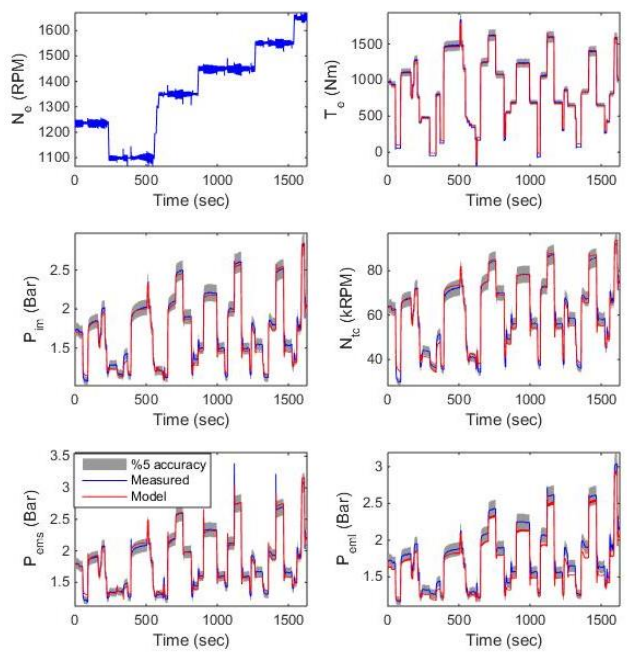

Figure 4- Model validation of the DD13 baseline engine.

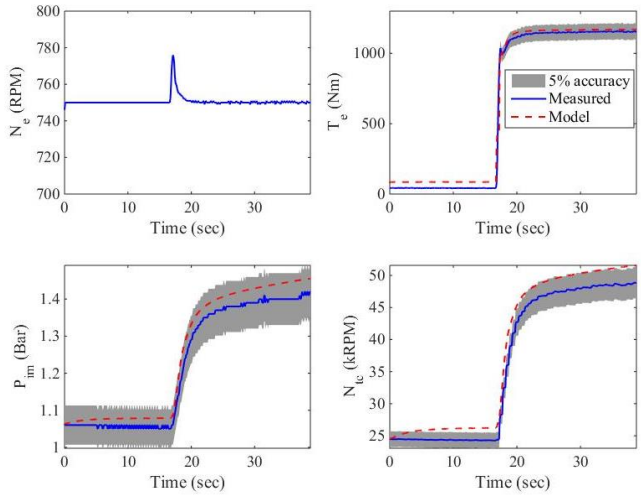

Figure 5- Load step (0-80%) validation of the DD13 engine model.

A water cooled eSC from Controlled Power Technologies (CPT) [10] is integrated into the engine model for evaluation of the eSC effect on engine torque response. The COBRA (COntrolled Boosting for Rapid response Applications) model C80 electric supercharger is comprised of a radial compressor (with the characteristic map shown in Figure 6) and a liquid cooled switched reluctance electric motor. An

electric bypass valve is also included in the model to bypass air around the eSC unit when this unit is off line.

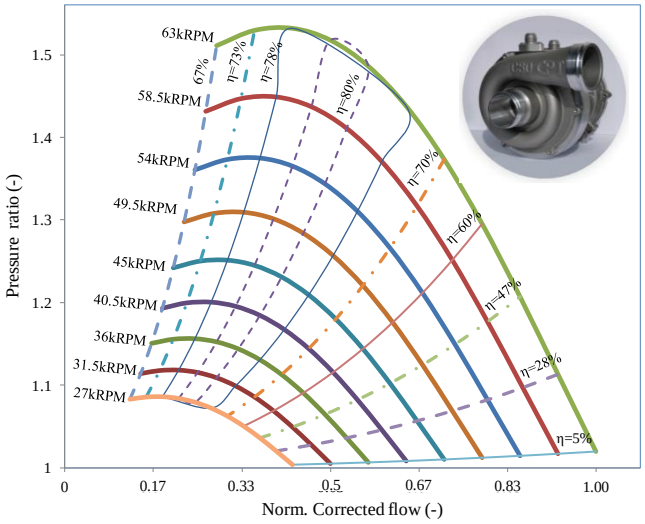

Figure 6-COBRA C80 compressor map.

Simple rule-based controllers are included in the model to coordinate the electric supercharger drive motor and the supercharger bypass valve. As shown in Figure 7, the controller applies a desired power to the electric motor ($PW_{d,esc}$) to speed up the eSC when a torque transient is detected ($\Delta T_e>0$) or the $\lambda=\lambda_{crit}$. For the bypass valve, the following hysteresis control strategy is used:

$$\theta_{valve}=\begin{cases}0 & \Delta P_{eSC}>\Delta^{+}_{Thr}\\ No\,change & \Delta^{-}_{Thr}<\Delta P_{eSC}<\Delta^{+}_{Thr}\\ 100 & \Delta P_{eSC}<\Delta^{-}_{Thr}\end{cases} \quad (1)$$

where the desired valve position (θ_{valve}) is calculated based on the difference between the upstream and downstream pressures of the eSC (ΔP_{eSC}) and upper and lower thresholds of the pressure difference ($\Delta^{-}_{Thr},\Delta^{+}_{Thr}$).

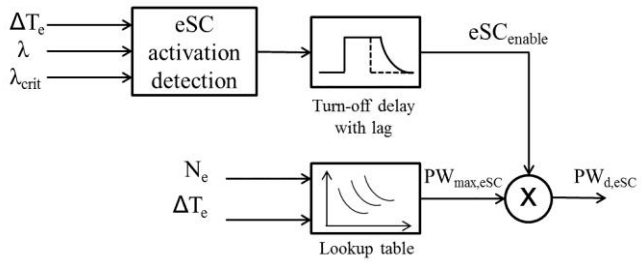

Figure 7- Strategy for control of the eSC electric motor power

BASELINE TC ENGINE POWER DISTURBANCE REJECTION

Engine speed dynamics are obtained from a power balance on the engine crankshaft:

$$\dot{N}_e=\frac{1}{N_e J_e}(PW_e-PW_{dist})$$
$$PW_e=PW_{ind}(\dot{m}_f,N_e,\lambda,\theta_{inj})-PW_p-PW_f. \quad (2)$$

In equation (2), PW_e is the engine brake power, PW_{ind} is the gross indicated power, PW_P is the pumping power loss, PW_f represents the friction power loss, J_e is the engine's moment of inertia, $\dot{m}_f$ is the fuel rate, and θ_{inj} is the injection phasing. As equation (1) suggests, increasing the power disturbance (PW_{dist}) reduces the engine speed if the engine power (PW_e) does not increase at the same rate as PW_{dist}. If the speed drops under some critical value, it would be commanded by the engine control module (ECM) to shut down the engine protecting it against the shaft's natural frequency and a potential lack of lubrication [12].

Operation of the HDD engine under a rapid rising power disturbance (PW_{dist}) is simulated in this section with results of N_e, PW_e , λ and the fuel limiter shown in Figure 8. Three different power increases are simulated from a near idle condition: 1) for a jump to PW_{dist}=85 kW with a fuel limiter threshold of λ_{crit}=1.6 2) PW_{dist}=85 kW and λ_{crit}=1.2 and 3) an even higher power jump to PW_{dist}=100kW and λ_{crit}=1.6. The PW_{dist}=85 kW corresponds to the engine full load at 608 RPM. In all of the test scenarios the power disturbance is applied as a ramp with $T_{0\text{-}100}$=100 ms. The engine is initially idling at 608 RPM as shown prior to the load ramp in Figure 8. When there is an abrupt microgrid power demand, the generator applies the corresponding torque (T_{dist}) to the engine in response to the demanded electrical power and consequently the engine speed droops. The engine speed controller observes the speed droop and increases the fuel command to increase the engine power/torque to maintain the desired speed. The injected fuel mass increases however this rate is limited by λ_{crit} (Figure 8- c and d) and ultimately the maximum allowable engine torque. This limitation reduces the rate of engine power/torque increase (Figure 8-b), causing the engine speed to decrease even more. As plots in Figure 8-a and c show, relaxing the λ_{crit} constraint from λ_{crit}=1.6 to λ_{crit}=1.2 allows an increase in injected fuel mass which increases the torque/power and consequently reduces the speed droop with the downside of increased small scroll exhaust manifold temperature (T_{ems}) as well as potential increase of smoke emissions. If the engine output power does not reach PW_{dist} then the engine speed reaches the minimum permissible value and the ECM shuts the engine down (as shown for the P_{dist}=100kW case in Figure 8-a). The

engine reaction to the applied power disturbance in the simulated test scenarios indicates a lack of air-charge during rapid transitions to high loads that finally could result in an engine stall. The fast air-charge increases with supercharging, specifically at low engine speeds is considered in this work as a means to mitigate the predicted engine speed droop.

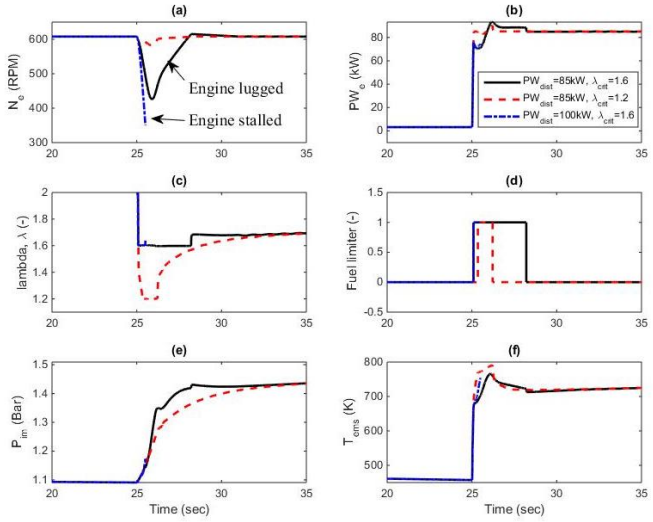

Figure 8- Baseline HDD engine response to different power ramps with $T_{0\text{-}100\%}$=10 ms.

SUPERCHARGED ENGINE AIR FLOW INCREASE

The eSC implementation increases the engine air charge to the cylinders (W_a). This is shown in Figure 9, as the maximum air flow into the engine with the eSC increases relative to the baseline TC engine, where:

$$\Delta W = \frac{W_{a,eSC} - W_{a,Base}}{W_{a,Base}} * 100 \qquad (3)$$

In equation (3), $W_{a,eSC}$ is calculated with the eSC at maximum power and with an injected fuel mass similar to the baseline engine. As the contour plot shows, in the lower left half of the map, the selected supercharger covers the lower half of the engine map with more than 50% air flow increase at low engine speeds. This advantage of supercharging increases the low-end torque compared to the baseline turbocharged engine that cannot provide sufficient air flow at low engine speeds (Figure 10). As shown in Figure 10, with the eSC integrated, the higher boost pressures enable increasing the low-end torque and flattening the torque curve while avoiding application of the fuel limiter for the avoidance of minimum lambda /high soot generation limits and the main compressor surge line. At high engine speeds (as Figure 10 shows) both the EGR valve and WG are open and can be used to increase the engine air-charge and torque, therefore supplementary boosting devices are not necessary. Moreover, large torque jumps happen at low engine speeds of military vehicles due to their stationary operation requirements.

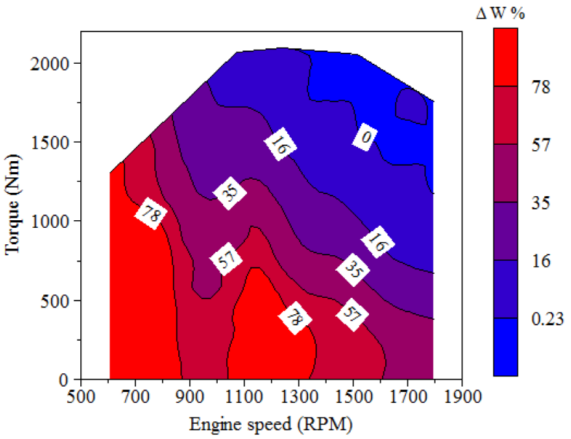

Figure 9- Percent increase in the engine air flow (ΔW) for the eSC engine relative to the baseline engine.

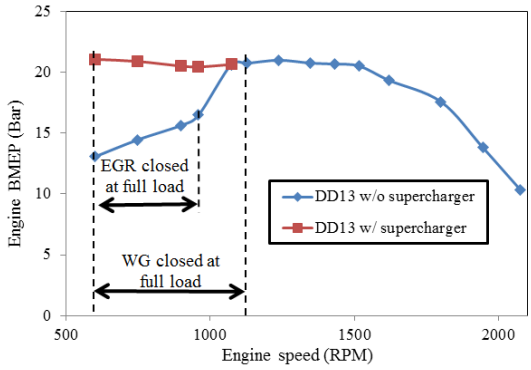

Figure 10- Improving the maximum low-end torque by using the eSC.

SUPERCHARGED ENGNE POWER DISTURBANCE REJECTION

The increase in engine air-charge with the eSC can improve the engine response time. A power disturbance the same as the test scenario in Figure 8 is applied to the engine to show how the eSC influences the engine response time. As Figure 11 shows, the supercharged engine speed drop decreases to ~ 23 RPM compared to a ~ 180 RPM drop in the baseline turbocharged engine speed. The increase in cylinder air-charge provided by the supercharger decreases engine fuel limited operation from ~ 3 seconds to less than 0.5 second (Figure 11-c) without relaxing the λ_{crit}=1.6 constraint (Figure 11-c) and increase of T_{ems}. The electrical power of the eSC (approximately 3.5 kW in Figure 11-d) can be provided by a conventional truck battery.

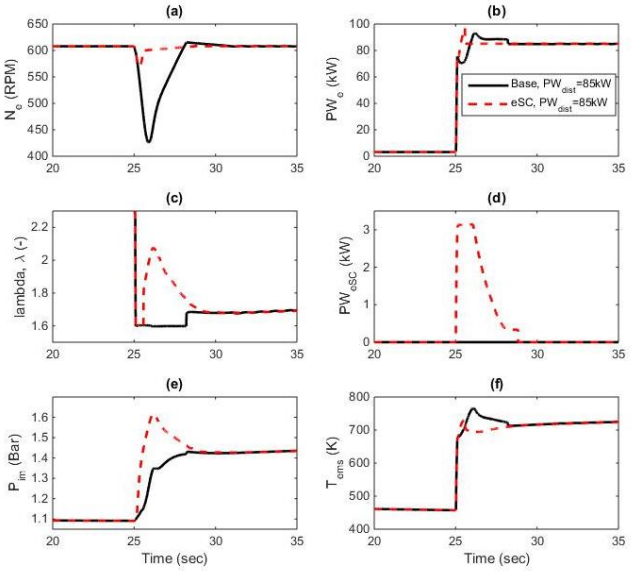

Figure 11- The effect of supercharging on engine response to a power disturbance.

Idle speed affects the air system response and crank shaft rotational inertia. It is possible that the variation of the idle speed will influence the ability of the engine to accept load. The idle speed effect is studied by examining three cases here. The first two are for the baseline engine, with increased idle speeds of 850 and 940 RPM (compared to the original 608 RPM) and the third one is the eSC engine without idle speed increase. In Figure 12 results are compared for a power disturbance of 100 kW applied to the engine over a 100 ms load ramp. For the eSC engine, the desired N_e is increased to 750 RPM after load application to avoid engine operation close to λ_{crit} after the transient, when the eSC goes offline. As shown in Figure 12, with idle speed elevated from 608 to 940 RPM, the baseline engine has sufficient initial air charge and rotational inertia in addition to fast dynamics so that it can reject the externally applied power disturbance with similar speed droop to the eSC engine. However the engine efficiency is reduced at 940 RPM through two mechanisms. First, the engine consumes more fuel by idling at higher speeds prior to load acceptance. Second, for a constant output power, increasing the speed reduces the engine torque. Since, generally, the engine BSFC increases as torque decreases, operation at lower torques and higher speeds (i.e. 940 RPM after load application in Figure 12-d) increases the BSFC. As shown in Figure 12, the eSC engine has a response time this is as fast as the engine with elevated idle speed, but without the sacrifice of efficiency. This fuel efficiency operation is of special importance at a tactical edge where supply of fuel is both difficult and dangerous[13].

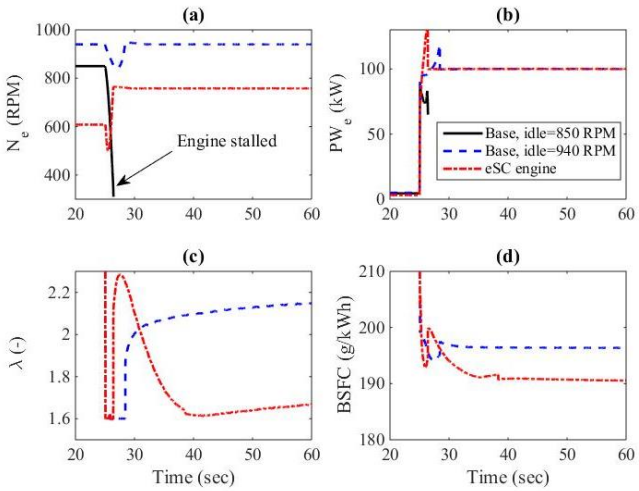

Figure 12- The effect of supercharging and increasing the engine idle speed on engine power response and BSFC. P_{dist}=100kW is applied to all tests and the eSC parasitic loss is included in the BSFC calculation.

CONCLUSIONS AND FUTURE WORK

This paper uses a mean value model to examine the ability of an electric supercharger (eSC) to improve the load acceptance of a 13 L DD13 heavy duty diesel (HDD) engine as it transitions from idle to near full load during a large microgrid power demand. Under steady state conditions at low speeds, which are key enablers for engine transient performance, the eSC was capable of increasing engine air mass flow rates by an average of 50%.

When subjected to an abrupt power demands, the eSC engine could quickly provide sufficient air to the cylinders to avoid engine smoke limits and the associated fuel limiter. On the other hand, the insufficient airflow and excessive fuel limiting of the baseline turbocharged engine resulted in lug, with a speed drop of 30% at 608 RPM. While the baseline engine idle speed could be increased to avoid such limits, the eSC approach results in up to 3.5% lower BSFC due to its final lower speed and higher load operation of the engine.

Fast increase of the engine power can have different solutions. Increasing the engine idle speed and supercharging are two cases studied in this paper. Reducing engine response time while minimizing fuel consumption are solutions of a path planning optimization problem for transitioning from low to high powers. This optimization along with optimal control of the supercharger speed are planned as future works.

REFERENCES

[1] Whitefoot JW, Mechtenberg AR, Peters DL, Papalambros PY. Optimal component sizing and forward-looking dispatch of an electrical microgrid for energy storage planning. ASME Paper No DETC2011-48513. 2011.

[2] Lopes JAP, Moreira CL, Madureira AG. Defining control strategies for MicroGrids islanded operation. IEEE Transactions on Power Systems. 2006;21:916-24.
[3] Waldron T, VanDyne E, Brown J. Improved Engine Performance and Efficiency Utilizing a Superturbocharger. DTIC Document; 2012.
[4] Newman P, Luard N, Jarvis S, Richardson S, Smith T, Jackson R, et al. Electrical supercharging for future diesel powertrain applications. In: Engineers IoM, editor. 11th International Conference on Turbochargers and Turbocharging. Oxford: Woodhead Publishing; 2014. p. 207-16.
[5] Khaligh A, Li Z. Battery, Ultracapacitor, Fuel Cell, and Hybrid Energy Storage Systems for Electric, Hybrid Electric, Fuel Cell, and Plug-In Hybrid Electric Vehicles: State of the Art. IEEE Transactions on Vehicular Technology. 2010;59:2806-14.
[6] Battery Performance Characteristics. http://www.mpoweruk.com/performance.htm2016.
[7] Salehi R, Stefanopoulou A. Effective Component Tuning in a Diesel Engine Model Using Sensitivity Analysis. ASME 2015 Dynamic Systems and Control Conference: American Society of Mechanical Engineers; 2015. p. V001T12A3-VT12A3.
[8] Hand MJ, Hellström E, Kim D, Stefanopoulou A, Kollien J, Savonen C. Model and Calibration of a Diesel Engine Air Path With an Asymmetric Twin Scroll Turbine. ASME 2013 Internal Combustion Engine Division Fall Technical Conference: American Society of Mechanical Engineers; 2013. p. V001T05A10-VT05A10.
[9] Salehi R, Stefanopoulou AG, Kihas D, Uchanski M. Selection and Tuning of a Reduced Parameter Set for a Turbocharged Diesel Engine Model. American Control Conference (ACC). Boston, USA2016.
[10] Salehi R, Martz J, Stefanopoulou A, Hansen T, Haughton A. Comparison of High- and Low-Pressure Electric Supercharging of a HDD Engine: Steady State and Dynamic Air-Path Considerations. SAE International; 2016.
[11] Stefanopoulou A, Smith R. Maneuverability and smoke emission constraints in marine diesel propulsion. Control Engineering Practice. 2000;8:1023-31.
[12] Tung SC, McMillan ML. Automotive tribology overview of current advances and challenges for the future. Tribology International. 2004;37:517-36.
[13] Ersal T, Ahn C, Peters DL, Whitefoot JW, Mechtenberg AR, Hiskens IA, et al. Coupling between component sizing and regulation capability in microgrids. Smart Grid, IEEE Transactions on. 2013;4:1576-85.

Nomenclature

N_e	Engine speed (RPM)
N_{tc}	TC speed (RPM)
PW_e	Engine power (kW)
PW_{dist}	Power disturbance from microgrid (kW)
P_{eml}	Large exhaust manifold pressure (Bar)
P_{ems}	Small exhaust manifold pressure (Bar)
P_{im}	Intake manifold pressure (Bar)
T_e	Engine torque (Nm)
T_{ems}	Small exhaust manifold temperature (K)
W_a	Engine fresh air (kg/s)
λ	Equivalence air fuel ratio (-)

Abbreviations

BSFC	Brake specific fuel consumption
EGR	Exhaust gas recirculation
EM	Electric motor
eSC	Electric supercharger
HDD	Heavy Duty Diesel
TC	Turbocharged
WG	Wastegate